Complexation, Phase Separation, and Redissolution in Polyelectrolyte−Macroion Solutions

Marie Skepö[†] and Per Linse*

Physical Chemistry 1, Center for Chemistry and Chemical Engineering, Lund University, P.O. Box 124, S-221 00 Lund, Sweden

Received April 23, 2002; Revised Manuscript Received September 11, 2002

ABSTRACT: The complexation, phase separation, and redissolution of polyelectrolyte−macroion solutions have been studied by means of Monte Carlo simulations. A simple model system with focus on the electrostatic interactions has been used to examine the properties of the macroion solutions at different amounts of oppositely charged polyelectrolytes. As oppositely charged polyelectrolytes are added, the stable macroion solution with repelling macroions becomes successively less stable. The strong electrostatic attraction brings macroions and polyelectrolytes closely together, and slightly before macromolecular charge equivalence, distinct and repelling complexes formed by macroions and polyelectrolytes are established. At macromolecular charge equivalence, the system becomes unstable, and a large and loose cluster of macroions and polyelectrolytes is formed. Finally, in excess of polyelectrolytes, the large cluster is broken up and the macroions are dispersed again—a redissolution has occurred. The effect of the macroion radius, the chain length, and the chain flexibility on the phase separation is also investigated. A semiflexible chain displayed a smaller tendency to promote phase instability as compared to flexible and stiff chains, the origin most likely arising from the similar chain persistence length and macroion radius.

1. Introduction

Polyelectrolytes are charged molecules that display a high solubility in water and strong adsorbing capacity on surfaces bearing an opposite charge. An interesting feature is that they can act both as a stabilizing and as a destabilizing agent in particle suspensions. The complexation of polyelectrolytes with oppositely charged macroions is therefore an essential ingredient in many technical and biological systems. Examples include synthetic polyelectrolytes adsorbing on colloidal particles,[1] surfactant micelles,[2] and proteins[3,4] as well as the complexation of DNA to latex particles,[5] dendrimers,[6] and proteins.[7,8] Applications of complexes made by synthetic polyelectrolytes and macroions include the control of dispersion stabilization, flocculation, and precipitation, while complexes made by charged biological polyelectrolytes and macroions are used for example the immobilization of enzymes and purification of proteins.

A frequent phenomenon in colloidal science is coacervation (liquid−liquid phase separation), in other words, an associative phase separation in which an aqueous solution of macromolecules of opposite charge separates into two immiscible liquid phases. The phase rich in macromolecules is referred to as the coacervate and is in equilibrium with another liquid phase poor in the macromolecules.[9−14] It is well-known from experiments that phase separation occurs when the polyelectrolyte charge-to-macromolecular charge ratio is close or identical to one. Redissolution of a polyelectrolyte−surfactant precipitate by using an excess of surfactant has frequently been observed.[15−20] For example, Thalberg and Lindman[17] investigated the system of the negatively charged polysaccharide hyaluronan and the cationic surfactant alkyltrimethylammonium bromide, while Carnali[20] focused on the phase diagram of the negatively charged surfactant tetradecyltrimethylammonium bromide (TTAB) and the positively charged polymer sodium polyacrylate. In both of these studies, phase separation at stoichiometric charge conditions and redissolution of the precipitate at excess of surfactant were observed. Moreover, Carnali[20] examined the redissolution in an excess of polymer.

Substantial theoretical effort has been devoted to the complexation of one or several macroions to a single polyelectrolyte. Generally, it has been shown that complexation between the polyelectrolyte and the macroion(s) occurs at sufficiently high linear charge density of the polyelectrolyte and charge of the macroion. A central aspect in the analytic studies by von Goeler and Muthukumar,[21] Gurovitch and Sens,[22] Park et al.,[23] and Mateescu et al.[24] has been the possibility to overcharge a spherical macroion by an oppositely charged polyelectrolyte. Moreover, Netz and Joanny[25] and Nguyen and Shklovskii[26] have used more detailed molecular models to examine the 1:1 complexation, and these systems have been subjected to simulations studies by Chodanowski and Stoll[27,28] and by Akinchina and Linse.[29] The complexation between one polyelectrolyte and several macroions has theoretically been addressed by Nguyen and Shklovskii[30] and Schiessel et al.[31] and by simulations by Jonsson and Linse.[32−34] Finally, the structure and phase behavior of polyelectrolyte−macroion solutions have been investigated by Ferreira et al.[35] employing liquid-state integral theory, Nguyen and Shklovskii[36] using phenomenological free energy expressions, and Harnau and Hansen[37] also utilizing liquid-state integral theory. In their study, Ferreira et al.[35] concluded from radial distribution functions an increased probability of finding macroions near each other in the presence of polyelectrolytes, and they also determined regions of phase instability. Nguyen and Shklovskii[36] presented phase diagrams and predicted aggregate formation in the vicinity of stoichiometric charge condi-

* E-mail: per.linse@fkem1.lu.se.
[†] Former last name Jonsson.

10.1021/ma020634l CCC: $25.00
Published on Web 12/19/2002

tions. Moreover, the charges of the aggregates at different conditions were also predicted. Harnau and Hansen[37] concluded an increased probability of having macroions close in space from radial distribution functions and reduced phase stability from structure factors at increasing electrostatic coupling in the system.

In this contribution, we address structural and phase properties of macroions solution with different amounts of oppositely charged polyelectrolytes by using Monte Carlo simulations. This study provides complementary results to the recent theoretical investigations in this area.[35−37] We employ a coarse-grained model with explicit representation of all charged species including the small ions as in our previous investigations of polyelectrolyte−macroion complexation.[32−34] Here, we observe the formation of a coacervate at macromolecular charge equivalence, and a redissolution of the phase separated system as further addition of polyelectrolytes was made. Just before charge equivalence smaller repelling clusters were found. Moreover, the effects of the macroion radius, the chain length, and the chain flexibility on the phase separation are also investigated. In particular, the relationship between the polyelectrolyte flexibility and curvature of the macroions was found to be important for the formation of larger clusters.

The outline of the paper is as follows. The model and some simulation aspects are given in section 2. In section 3, the results are presented and discussed, and the paper ends with conclusions given in section 4.

2. Model and Method

2.1. Model. Solutions containing macroions and different amounts of oppositely charged polyelectrolytes are described using the primitive model. In this approach, charged hard spheres varying in charge and in size represent the ionic particles, whereas the solvent enters the model only through its permittivity. The model contains four different types of charged particles: (i) connected spheres representing hydrophilic linear polyelectrolytes, (ii) large unconnected spheres representing macroions, (iii) small unconnected spheres representing small positive ions (cations), and (iv) small unconnected spheres representing small negative ions (anions). The polyelectrolytes are described as freely jointed chains of charged hard spheres (segments) connected by harmonic bonds with their intrinsic chain flexibility regulated by harmonic angular energy terms.

The total potential energy of the system is given by

$$U = U_{\text{nonbond}} + U_{\text{bond}} + U_{\text{angle}} \tag{1}$$

where the nonbonded energy is assumed pairwise additive according to

$$U_{\text{nonbond}} = \sum_{i<j} u_{ij} \tag{2}$$

Within the primitive model, the interaction potential u_{ij} for pair ij, where i and j denote either a polyelectrolyte segment (seg), a macroion (M), a cation, or an anion, is given by

$$u_{ij}(r_{ij}) = \begin{cases} \infty & r_{ij} < R_i + R_j \\ \dfrac{Z_i Z_j e^2}{4\pi\epsilon_0\epsilon_r}\dfrac{1}{r_{ij}} & r_{ij} \geq R_i + R_j \end{cases} \tag{3}$$

where Z_i is the charge of particle i, R_i the radius of particle i, e the elementary charge, ϵ_0 the permittivity of vacuum, ϵ_r the permittivity of water, and $r_{ij} \equiv |\mathbf{r}_j - \mathbf{r}_i|$ the distance between the centers of particles i and j with $\mathbf{r}_i$ denoting the position of particle i. The permittivity is constant throughout the system, and hence surface polarization is neglected.

Table 1. Parameters of the Reference System

box length	$L = 257.92$ Å
macroion radius	$R_M = 15$ Å
segment radius	$R_{seg} = 2$ Å
small ion radius	$R_{ion} = 2$ Å
macroion charge	$Z_M = -10$
segment charge	$Z_{seg} = 1$
small ion charge	$Z_{ion} = \pm 1$
no. of polyelectrolytes	$N_{pe} = 0, 1, 2, 4, 8, 10, 15, 20$
no. of segments	$N_{seg} = 20$
no. of macroions	$N_M = 20$
no. of cations	$N_{cation} = 200$
no. of anions	$N_{anion} = 20-400$
temperature	$T = 298$ K
relative permittivity	$\epsilon_r = 78.4$

The remaining two terms in eq 1 are the bond and the angular energy potentials, which applies only to the polyelectrolyte. The bond energy is given by

$$U_{\text{bond}} = \sum_{i=1}^{N_{\text{seg}}-1} \frac{k_{\text{bond}}}{2}(r_{i,i+1} - r_0)^2 \tag{4}$$

where $r_{i,i+1}$ denotes the distance between two connected segments with the equilibrium separation $r_0 = 5$ Å and the force constant $k_{\text{bond}} = 0.4$ N/m and where N_{seg} denotes the number of segments of the polyelectrolyte. When all interactions are included, the root-mean-square (rms) segment−segment separation $\langle R_{\text{seg,seg}}^2\rangle^{1/2}$ was typically 6.0 Å. The angular energy is represented by

$$U_{\text{angle}} = \sum_{i=2}^{N_{\text{seg}}-1} \frac{k_{\text{ang}}}{2}(\alpha_i - \alpha_0)^2 \tag{5}$$

where α_i is the angle formed by the vectors $\mathbf{r}_{i+1} - \mathbf{r}_i$ and $\mathbf{r}_{i-1} - \mathbf{r}_i$ made by three consecutive segments with the equilibrium angle $\alpha_0 = 180°$ and the force constant k_{ang}. In addition to the angular potential, the electrostatic interaction among the segments also contributes to the rigidity of the polyelectrolyte, and this electrostatic contribution is of course affected by other ionic particles.

We will consider the properties of a reference system and the effect of systematic changes of it. The reference system contains $N_M = 20$ macroions, $N_{pe} = 0-20$ polyelectrolytes, and their counterions. A macroion has the radius $R_M = 15$ Å and the charge $Z_M = -10$, whereas a polyelectrolyte has $N_{seg} = 20$ segments, a segment having the radius $R_{seg} = 2$ Å and possessing one elementary charge $Z_{seg} = 1$, making the polyelectrolyte charge $Z_{pe} = N_{seg}Z_{seg} = 20$. An angular force constant $k_{ang} = 0$ is used, leading to a bare persistence length of $l_p = 7$ Å. The charged species are enclosed in a cubic box with the length L. If nothing else is stated, $L = 258$ Å, which is equivalent to a macroion volume fraction $\phi_M = (4\pi/3)R_M^3\rho_M = 0.0165$ with $\rho_M = N_M/L^3$. Throughout, $T = 298$ K and $\epsilon_r = 78.4$ are used, thus representing water at ambient temperature. Parameters of the reference system are compiled in Table 1.

In addition to the reference system, systems with different (i) macroion size R_M, (ii) polyelectrolyte length

N_{seg}, and (iii) bare chain persistence length l_p have been investigated. In (i) the macroion Z_M charge was held constant, in (ii) the total number of polyelectrolyte segments $N_{pe}N_{seg}$ was kept constant by a concomitant change of the number of chains in the system N_{pe}, and in (iii) the bare chain persistence length was increased by using $k_{ang} > 0$ (same values as in ref 33 was used).

The bare persistence length was calculated according to $l_p = \langle R_{seg,seg}^2\rangle^{1/2}/(1 + \langle\cos\alpha_i\rangle)$ (see ref 29 for a comparison of different methods to evaluate l_p) for the corresponding uncharged and isolated chain. The fact that $l_p > \langle R_{seg,seg}^2\rangle^{1/2}$ for $k_{ang} = 0$ is due to a slight stretching of the chain arising from the hard-sphere repulsion between the chain segments.

An important parameter characterizing the present systems is the stoichiometric polyelectrolyte charge-to-macroion charge ratio $\beta \equiv |N_{pe}Z_{pe}|/|N_MZ_M|$. This ratio ranges from 0 ($N_{pe} = 0$) to 2 ($N_{pe} = 20$) where the number of chains given is for the reference system. In particular, the charge ratio $\beta = 1$ denotes a system with equal amount of polyelectrolyte and macroion charges, also referred to as macromolecular charge equivalence.

2.2. Simulation Aspects. The equilibrium properties of the model systems were obtained from canonical Monte Carlo (MC) simulations according to the Metropolis algorithm.[38] The particles were enclosed in a cubic box, and periodical boundary conditions were applied. The long-ranged Coulomb interactions were handled by using the Ewald summation technique with conduction boundary conditions (see ref 32 for further details). The examination of the configurational space was accelerated by using four different types of displacements of the polyelectrolyte: (i) translational displacement of single charged particle, (ii) pivot rotation of a part of the polyelectrolyte chain, (iii) translation of the entire polyelectrolyte chain, and (iv) slithering move.[39] The probabilities of different trial moves were selected to enable single-particle moves 20 times more often than the pivot movements and the translations of the entire chain and 10 times more often than the slithering movements. The particles were initially placed randomly in the simulation box, and after equilibrium of typical 1×10^5 MC passes (trial moves per particle), a production run comprising in general 2×10^5 MC passes was performed.

Despite the strong polyelectrolyte−macroion attraction, it has previously been shown that the present protocol produces a satisfactorily sampling for a system containing one polyelectrolyte and several macroions.[32,33] In particular, the probability of a macroion to complex to different segments of the polyelectrolyte was examined. With the use of these probability functions, it was concluded that (i) in systems with a small number of macroions, in which all macroions were simultaneously complexed to the polyelectrolyte, frequent exchanges among the macroion with different positions along the chain contour occurred, and (ii) in systems with an excess of macroions, frequent exchanges between complexed and free macroions appeared.

These examinations have here been complemented by considering rms displacements and a residence "time" correlation function $\psi(n_{MC})$. The rms displacements of the polyelectrolyte segments and macroions during the production runs of the reference system at $\beta = 0$, 0.8, 1, and 2 are given in Table 2. In all cases and for both types of macromolecules, the rms displacements were at least half of the box length ($L = 258$ Å) and much larger than typical correlation lengths in the systems. The residence "time" correlation function $\psi(n_{MC})$ provides information on how long (measured in number of MC passes) a macroion is complexed to a given polyelectrolyte. More formally, $\psi(n_{MC})$ denotes the fraction of initially present binary polyelectrolyte−macroion complexes which remains (or have been reformed) after n_{MC} MC passes. Figure 1 displays $\psi(n_{MC})$ for the reference system at $\beta = 1$, a condition at which the system displays a formation of a large cluster (see Figure 2c). It is observed that $\psi(n_{MC})$ decays nearly exponentially, and a decay time of $\approx 0.8 \times 10^5$ MC passes is obtained after taking account the limiting value of $\psi(n_{MC} \rightarrow \infty) \approx 0.3$ (on average three of the 10 polyelectrolyte chains are complexed to a given macroion). The residence "time" is hence ≈40% of the production run, demonstrating frequent formations and disruptions of binary polyelectrolyte−macroion complexes. Thus, both the rms displacements and the correlation analysis strongly indicate that the present simulations are not trapped in only a subsection of the relevant part of the configurational space.

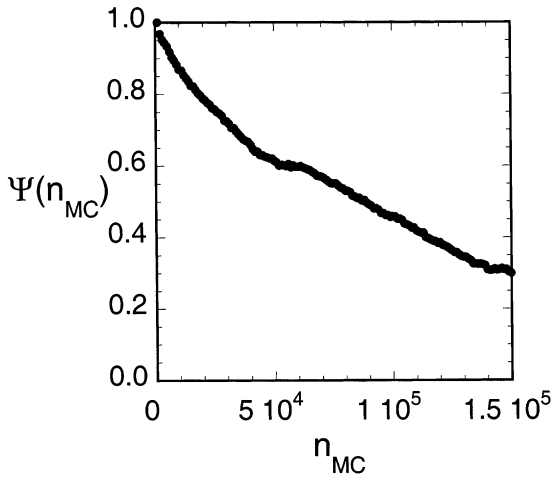

Figure 1. Residence "time" correlation function $\psi(n_{MC})$ vs the number of MC passes n_{MC} for the reference system at $\beta = 1$. The function expresses the probability that a polyelectrolyte remains complexed to a given macroion after n_{MC} MC passes given that the polyelectrolyte initially was complexed to that macroion. A polyelectrolyte is considered to be complexed to a macroion if at least one of its segments is within 22 Å from the center of the macroion (cf. the contact distance of 17 Å). Formally, $\psi(n_{MC}) = \langle\chi(0)\chi(n_{MC})\rangle$, where $\chi(n_{MC}) = 1$ if the polyelectrolyte still is complexed to a given macroion after n_{MC} MC passes; otherwise $\chi(n_{MC}) = 0$, and $\langle\ldots\rangle$ denotes an average over the macroions and initial points.

Table 2. Rms Displacements (in Å) of Polyelectrolyte Segments and Macroions at Different Stoichiometric Charge Ratios of the Reference System

β	segments	macroions
0		420
0.8	140	180
1	180	160
2	210	190

The reported uncertainty of simulated quantities is one standard deviation of the mean. It is estimated from the deviation among the means of the subdivisions of the total number of MC passes according to

$$\sigma^2(\langle x\rangle) = \frac{1}{n_s(n_s - 1)}\sum_{s=1}^{n_s}(\langle x\rangle_s - \langle x\rangle)^2 \qquad (6)$$

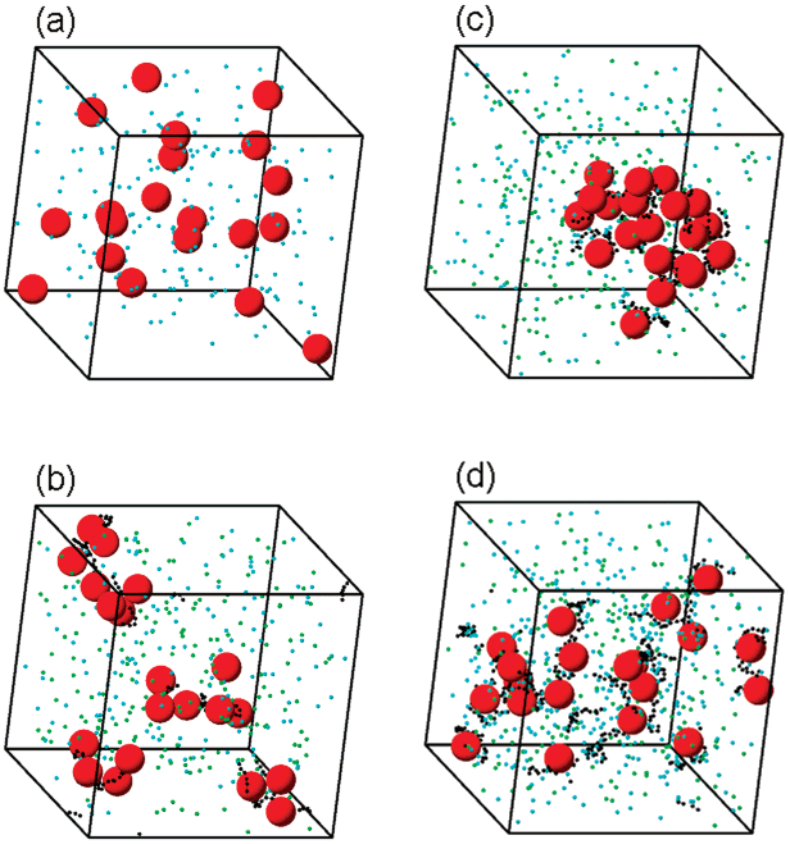

Figure 2. Typical configurations of a macroion solution containing variable amounts of oppositely charged polyelectrolytes. The simulated system contains 20 macroions (large red spheres) and (a) $N_{pe} = 0$, (b) 8, (c) 10, and (c) 20 polyelectrolytes with 20 segments (black dots), which corresponds to a polyelectrolyte charge-to-macroion charge ratio $\beta = 0$, 0.8, 1, and 2, respectively. The green and blue dots are the small positive and negative ions. The length of the box edge is 258 Å, and particles are drawn to scale. Periodic boundary conditions are applied in all three directions to avoid surface artifacts.

where $\langle x \rangle_s$ is the average of quantity x from one subdivision, $\langle x \rangle$ the average of x from the total simulation, and $n_s = 10$ the number of subdivisions.

The simulations were performed by using the integrated Monte Carlo/molecular dynamics/Brownian dynamics simulation package Molsim.[40]

2.3. Structural Analysis. Structure factors (sf's) and radial distribution functions (rdf's) have been used to characterize the structure of the solutions.

The structure factor $S(q)$ of a system containing N scattering objects is defined by

$$S(q) = \left\langle \frac{1}{N} \left| \sum_{j=1}^{N} \exp(i\mathbf{q}\cdot\mathbf{r}_j) \right|^2 \right\rangle \tag{7}$$

For a multicomponent system the partial structure factor $S_{ij}(q)$, involving N_i objects of type i and N_j of type j, is defined analogously according to

$$S_{ij}(q) = \left\langle \frac{1}{(N_i N_j)^{1/2}} \left[\sum_{i=1}^{N_i} \exp(i\mathbf{q}\cdot\mathbf{r}_i) \right] \left[\sum_{j=1}^{N_j} \exp(-i\mathbf{q}\cdot\mathbf{r}_j) \right] \right\rangle \tag{8}$$

and $S(q)$ and the set $\{S_{ij}(q)\}$ are related through

$$S(q) = \sum_{i=1}^{N_i} \sum_{j=1}^{N_j} \frac{(N_i N_j)^{1/2}}{N} S_{ij}(q) \tag{9}$$

Sometimes the factor $(N_i N_j)^{1/2}/N$ is trivially shifted from eq 9 to eq 8. For a periodic system with length L, $q < 2\pi/L$ is not accessible. Numerically, the partial structure factors were evaluated using eq 8.

The structure factor is useful for assessing the stability of a system. An increase of the magnitude of S as q approaches zero implies an appearance of density fluctuations at long length scales. Obviously, in a finite system $S(q\rightarrow 0)$ always remains finite. However, in the thermodynamic limit, $S(q\rightarrow 0)$ diverges as the system becomes intrinsically unstable at the spinodal curve, whereas $S(q\rightarrow 0)$ grows but remains finite as the system becomes metastable at the bimodal curve. The isothermal compressibility of a system is proportional to $S(q=0)$.

The radial distribution function $g_{ij}(r)$ measures the spatial correlations in the real space. It expresses the relative density of a particle of type j at a distance r from a given particle of type i. At short distance $g_{ij}(r)$ is zero because of hard-sphere overlap, whereas in a homogeneous solution $g_{ij}(r)$ conventionally approaches one at large r. Numerically, $g_{ij}(r)$ was obtained by sampling the frequency at which particles of type i and j were separated by the distance r.

The partial structure factor $S_{ij}(q)$ and the rdf $g_{ij}(r)$ are related according to $S_{ij}(q) = \delta_{ij} + (\rho_i \rho_j)^{1/2} H_{ij}(q)$, where δ_{ij} is the Kronecker delta and $H_{ij}(q)$ a 3-dimensional Fourier transform of the total correlation function $h_{ij}(r) = g_{ij}(r) - 1$. Despite the fact that sf's and rdf's are related to each other, the two quantities emphases partly different aspects of the structure.

3. Results and Discussion

3.1. Reference System. The properties of the reference system consisting of a solution of macroions with different amounts of oppositely charged polyelectrolytes will first be considered.

3.1.1. Overview. Typical configurations of the macroion solutions with 0, 8, 10, and 20 polyelectrolytes corresponding to the stoichiometric charge ratios β = 0, 0.8, 1, and 2, respectively, are displayed in Figure 2. The snapshots indicate that in the pure macroion solution ($\beta = 0$) the macroions are well separated, forming a homogeneous solution. After an addition of polyelectrolytes, but still having a solution with a deficiency of polyelectrolyte charges ($\beta = 0.8$), distinct complexes of macroions and polyelectrolytes appear. At macromolecular charge equivalence ($\beta = 1$), essentially a large and loosely packed cluster is formed. Finally, with an excess of polyelectrolyte charges ($\beta = 2$), the large cluster is redissolved, and the macroions become to a large extent separated again.

3.1.2. Structure. The macroion−macroion, macroion−segment, and segment−segment sf's at different stoichiometric charge ratios are provided in Figure 3. In Figure 3a and starting with a pure macroion solution ($\beta = 0$), $S_{MM}(q)$ displays a maxima at ≈0.095 Å^{-1} corresponding to typical macroion−macroion separations ≈ $2\pi/0.095$ = 66 Å. The small amplitude of S_{MM} at small q implies small density fluctuations at long length scales. Hence, typical features of a homogeneous solution of a charge stabilized macroion solution are obtained. Upon addition of polyelectrolytes, the general trend is that $S_{MM}(q)$ at small q grows until macromolecular charge equivalence ($\beta = 1$) is achieved, whereas further addition of polyelectrolytes makes $S_{MM}(q)$ at small q to attain smaller values again. The large magnitude of $S_{MM}(q)$ at small q for $\beta = 1$ demonstrates large density fluctuations at long length scales and implies an unstable solution. The reduction of $S_{MM}(q)$ at small q for $\beta > 1$ demonstrates an increased stability of the solution. We also notice that at $\beta = 0.4$ and 2.0, with nearly the same relative deviations from $\beta = 1$, the macroion−macroion structure factors are almost identical. Finally, at $\beta = 0.8$, $S_{MM}(q)$ displays a maximum at $q \approx 0.04$ Å^{-1}, indicating complexes well separated, presumably by repulsive electrostatic interactions.

Figure 3b shows the corresponding macroion−segment sf's. The appearance of $S_{M,seg}(q)$ at small q resembles closely that of $S_{MM}(q)$. Thus, the spatial macroion−segment correlations are similar to the macroion−macroion correlations, signifying a strong spatial coupling between the macroions and the polyelectrolyte segments.

Finally, Figure 3c displays the sf's between polyelectrolyte segments $S_{seg,seg}(q)$ on a log−log representation, clearly illustrating the sf at larger q. For all β, $S_{seg,seg}(q)$ displays the same feature at $q = q' \approx 1.0$ Å^{-1} arising from two segments directly bonded with the rms segment−segment separation ≈6.0 Å. At smaller q, $S_{seg,seg}(q)$ scales as $q^{-1/\nu}$ with the Flory exponent $\nu \approx 0.84$, demonstrating that the chains are substantially stretched ($\nu = 0.5$ for a Gaussian chain and $\nu = 1$ for a rod). At $q < 0.05$ Å^{-1}, $S_{seg,seg}(q)$ becomes dependent on β in a similar fashion as $S_{MM}(q)$ and $S_{M,seg}(q)$, but less visible due to the log−log scale.

The corresponding rdf's are provided in Figure 4. At $\beta = 0$, the macroion−macroion rdf's displayed in Figure

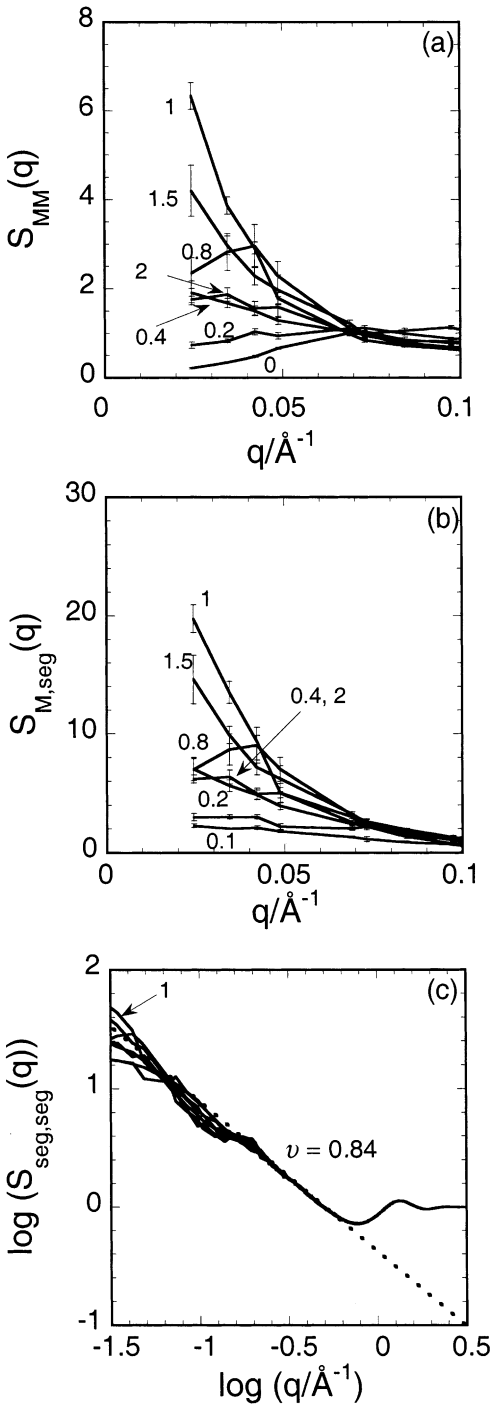

Figure 3. (a) Macroion−macroion structure factors $S_{MM}(q)$, (b) macroion−polyelectrolyte segment structure factors $S_{M,seg}(q)$, and (c) the polyelectrolyte segment−segment structure factors $S_{seg,seg}(q)$ in log−log representation of the reference system at indicated stoichiometric charge ratio β.

4a also reveal typical features of a charged stabilized solution of macroions: (i) low probability of finding macroions in contact with each other, $g_{MM}(2R_M = 30$ Å) ≈ 0, and (ii) a first maximum roughly at $\rho_M^{-1/3} \approx 80$ Å (not fully visible in Figure 4a). Upon addition of oppositely charged polyelectrolytes, a maximum in $g_{MM}(r)$ occurs at $r \approx 37$ Å, demonstrating an increased probability of macroions being close to each other. The largest amplitude of this maximum appears at macromolecular charge equivalence, $\beta = 1$, whereas at $\beta > 1$ the amplitude of the maxima decreases as β is increased. At $\beta = 2$, a significant maximum still appears, showing

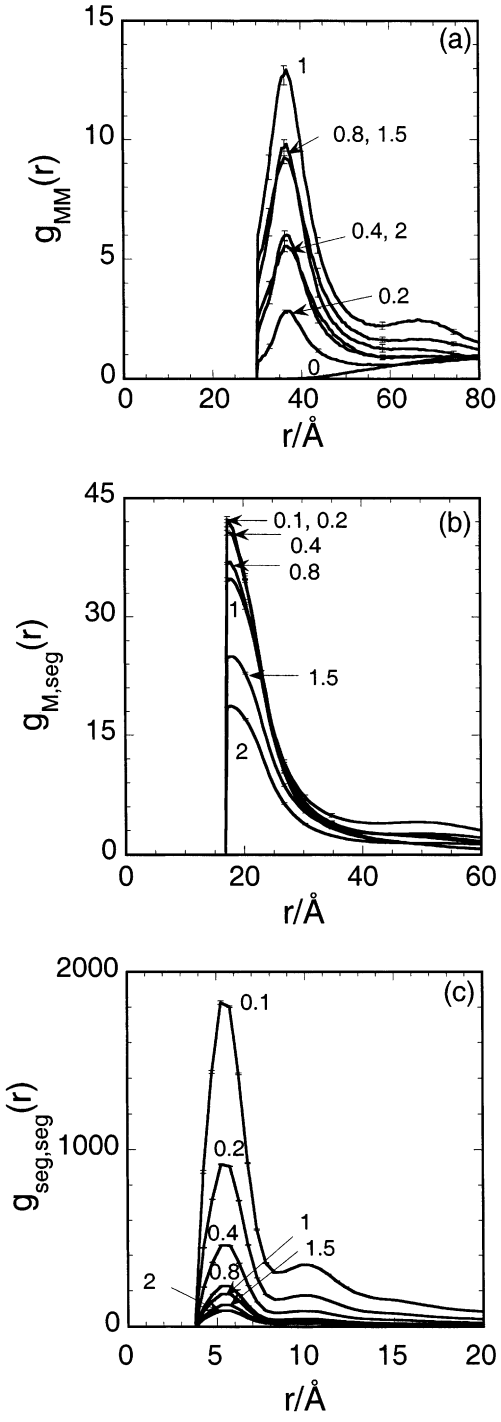

Figure 4. (a) Macroion−macroion radial distribution functions $g_{MM}(r)$, (b) macroion−polyelectrolyte segment radial distribution functions $g_{M,seg}(r)$, and (c) the polyelectrolyte segment−segment radial distribution functions $g_{seg,seg}(r)$ of the reference system at indicated stoichiometric charge ratio β.

a remaining macroion pairing. Moreover, at $0.4 \leq \beta \leq 2$ and in particular at $\beta = 1$, a second broad maximum occurs at $r \approx 70$ Å, indicating a buildup of larger macroion clusters involving a second layer of macroions. The location of the maximum at $r \approx 37$ Å is insensitive to β, showing that macroion pairing mediated by intervening polyelectrolyte is governed by short-range correlations. However, as the macroions charge, segment charge, or chain stiffness is changed, the location of this maximum is shifted.[32,33]

Figure 4b shows the macroion−segment rdf's, $g_{M,seg}(r)$. At all conditions, a pronounced maximum appears at the contact separation $r = R_M + R_{seg} = 17$ Å. The width of the polyelectrolyte layer around the macroions is ≈10 Å. The magnitude of the maximum decreases as more polyelectrolytes are added (increased β) due to a more homogeneous distribution of the polyelectrolyte segments in the solution with respect to a given macroion. At $\beta = 1$, $g_{M,seg}(r)$ displays an additional broad maximum at $r \approx 50$ Å, again demonstrating the presence of extended clusters.

Table 3. Average Number of Clusters, the Composition, and the Probability of the Most Frequent Clusters at Different Stoichiometric Charge Ratios of the Reference System[a]

β	$\langle N_{cluster} \rangle$	composition (N^c_{pe}, N^c_M)	probability
0	20	(0, 1)	1.0
0.8	5.0	(0, 1), (1, 3), (2, 4), (1, 2)	0.262, 0.253, 0.154, 0.114
1	2.9	(1,2), (9,18)	0.362, 0.111
2	6.6	(1,1), (1,0), (2,2)	0.337, 0.141, 0.128

[a] See text for the definition of a cluster.

The polyelectrolyte segment−segment rdf's are displayed in Figure 4c. The two most prominent features displayed, in particular at low β, are the maxima at $r \approx 5.5$ and 10 Å, arising from two segments directly bonded or bonded through a common neighbor, respectively. The appearance of two such distinct distributions with the ratio of their locations near 2 shows that the polyelectrolyte is locally stretched. The reduction of the amplitude of $g_{seg,seg}$ as β is increased arises again from the increase of the polyelectrolyte density.

Figure 2 showed that macromolecules form clusters, and the degree of cluster formation depends on β. The composition (number of macroions and polyelectrolytes) and the probability of clusters formed have been analyzed. Two macromolecules (macroion or polyelectrolyte) were considered to belong to the same cluster if they were "connected" directly or indirectly through one or several other macromolecules. Two macroions were directly connected if $r_{MM} \leq 45$ Å, a macroion and a polyelectrolyte were directly connected if for any segment $r_{M,seg} \leq 22$ Å, and two polyelectrolytes were directly connected if for any pair of segments $r_{seg,seg} \leq 10$ Å was fulfilled (cf. their hard-sphere radii R_i). The definition of connected macromolecules is somewhat arbitrary, but the trends obtained are not sensitive on the exact geometrical definitions. The result of the cluster analysis is given in Table 3. It should be noted that the probabilities refer to the appearance of clusters of a given composition; the probabilities of finding macromolecules in clusters of given compositions are different (cf. number and mass weighted averages).

The general trend is that the average number of clusters formed $\langle N_{cluster} \rangle$ is decreasing until $\beta = 1$, and then it starts to increase again. For $\beta = 0$ each macroion on its own constitutes a cluster consistent with the macroion−macroion rdf shown in Figure 4a. For $\beta = 0.8$ there is on the average 5.0 clusters, and they either are neutral or possess an excess of macroion charges. When $\beta = 1$, $\langle N_{cluster} \rangle$ has decreased to 2.9, and the majority of the macromolecules reside in one large cluster consisting of 9 polyelectrolytes and 18 macroions. In an excess of polyelectrolytes ($\beta = 2$), $\langle N_{cluster} \rangle = 6.6$ and the clusters now possess an excess of polyelectrolyte charges.

The sf's, the rdf's, and the cluster analysis (i) are throughout consistent with the picture provided by the snapshots given in Figure 2 and (ii) quantifies the

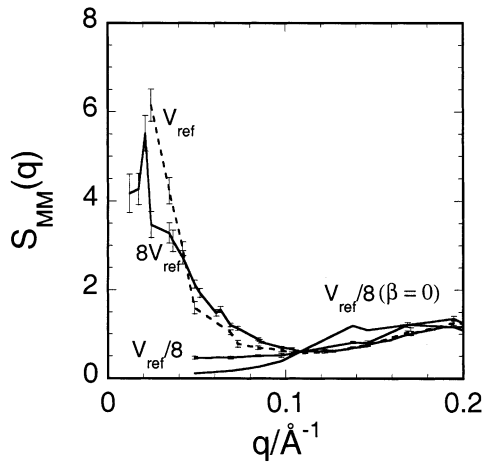

Figure 5. Macroion−macroion structure factors $S_{MM}(q)$ at $\beta = 0$ and $\beta = 1$ of the reference system at indicated solution volume V.

structures of the solutions. Thus, as oppositely charged polyelectrolytes are added, the initially homogeneous macroion solution with repelling macroions becomes successively more inhomogeneous as clusters of polyelectrolytes and macroions are formed. The strong electrostatic attraction brings macroions and polyelectrolytes closely together, and as a consequence the like-charged macroions have a high probability to become near each other in space. Slightly before the macromolecular charge equivalence $\beta = 1$, distinct and repelling complexes formed by macroions and polyelectrolytes are established. At $\beta = 1$, the system becomes unstable, and a large and loosely packed cluster of macroions and polyelectrolytes is formed. Finally, in excess of polyelectrolytes, the large cluster is broken up, and the macroions are dispersed again. Our findings suggest that in the thermodynamic limit the following sequence of events appears as polyelectrolyte is added to a dilute charge-stabilized macroion solution: stable and homogeneous macroion solution → formation of macroion−polyelectrolyte complexes in a still stable solution → a separation into two phases, one rich in the macromolecules and one poor in them, → a redissolution resulting in a single and stable macroion−polyelectrolyte solution.

3.1.3. Partial Phase Map. As shown, the reference system becomes unstable and displays a phase separation about $\beta = 1$. We will now consider the phase stability at fixed β ($\beta = 1$), but at variable density. Experimentally, ternary phase diagrams show that a phase-separated system becomes a one-phase at sufficiently low water content. Upon dilution, the region of the two-phase region extends very close to the water corner of the ternary phase diagram.[18] Typically, only when the electrostatic attraction between the oppositely charged macromolecules is attenuated does the two-phase region detach from the water corner.[41]

At the stoichiometric charge ratio $\beta = 1$, macroion−macroion sf's have been determined at several solution volumes V ranging from $V_{ref}/8$ to $8V_{ref}$, where $V_{ref} = L_{ref}^3$, with $N_M = 20$. A selection of macroion−macroion sf's at different V is displayed in Figure 5. At $V = V_{ref}/8$, $S_{MM}(q)$ has similar shape as that at $\beta = 0$ and $V = V_{ref}$ (cf. curves labeled $V_{ref}/8$ in Figure 5 and labeled 0 in Figure 3a) with the obvious length rescaling $q \rightarrow 2q$; hence, we have a homogeneous and stable solution. [Figure 5 also displays $S_{MM}(q)$ for $\beta = 0$ at $V_{ref}/8$, and the larger amplitude at small q for $\beta = 1$ as compared to $\beta = 0$ nevertheless implies that the polyelectrolytes induces a somewhat larger density fluctuations of the macroions.] Moreover, since the large cluster appearing at $V = V_{ref}$ (see Figure 2c) has a diameter of $\approx L_{ref}/2$, it is conceivable that the solution becomes homogeneous at $L = L_{ref}/2$. The 8-fold dilution from $V = V_{ref}$ to $8V_{ref}$ leads to a slight reduction of the density fluctuations at small q, but the solution is still inhomogeneous and unstable. Examination of even more dilute systems became computationally too demanding.

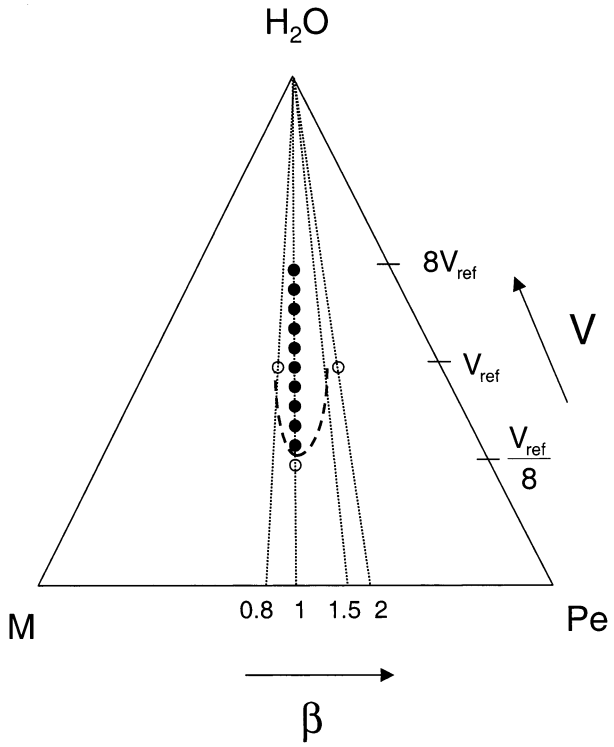

Figure 6. Partial ternary phase map of the reference system composed of macroions, polyelectrolytes, and water. The number of macroions was held fixed, whereas the stoichiometric charge ratio β represents the relative amount of polyelectrolytes and the solution volume V (note the logarithmic scale) represents the relative amount of water. Open circles denote one-phase systems, filled circles denote two-phase systems, and the dashed curve indicates a part of the border between one-phase and two-phase regions.

The results of the solution stability at different V for $\beta = 1$ and at different β for $V = V_{ref}$ are summarized in Figure 6 through a partial ternary phase map (note the logarithmic V scale). This (conventional) representation of the phase behavior clearly demonstrates that the instability region appears near the stoichiometric charge ratio $\beta = 1$ and that it extends over a considerable range of the concentration of the macromolecules. It agrees qualitatively with experimental observations, where the complex formation between oppositely charged macromolecules is electrostatically driven.[12] In particular, (i) the extension of the two-phase region along the $\beta = 1$ line, (ii) the termination of the two-phase region in concentrated solutions, and (iii) the extension of the two-phase region in practice to the water corner are three characteristic features displayed by the present model system.

3.1.4. Osmotic Pressure and Role of Counterions. In a solution containing highly charged macromolecules and their counterions, the counterions are electrostatically attracted by the charged macromolecules, and they are to a large degree located near the surfaces of the charged

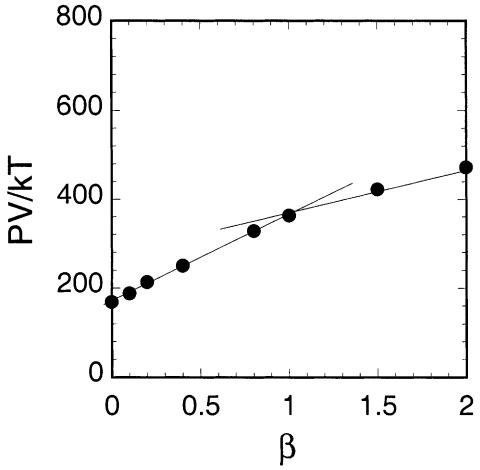

Figure 7. Pressure vs the stoichiometric charge ratio for the reference system.

macromolecules. The electrostatic attraction gives rise to an osmotic pressure P smaller than the pressure of the corresponding ideal system $P_{ideal} = \rho kT$ with ρ being the number density of the solution. When oppositely charged macromolecules are mixed, counterions accumulated near the macromolecules are released and become more homogeneously distributed in the solution.

In our previous contribution,[32] the distribution of the small ions with respect to the macroions and the polyelectrolyte segments was examined. The results supported the notion of a more homogeneous distribution of the small ions, as oppositely charged macroions are complexed. The corresponding analysis of the reference system at different β (data not shown) provided the same picture.

The thermodynamic consequences of the accumulation/release of the counterions to/from the charge macromolecules have also been examined. Figure 7 shows the pressure given as a function of the amount of polyelectrolyte in the macroion solution, again expressed by β. The pressure increases linearly with the amount of polyelectrolytes added, but the increase displays two regions with different slopes. In the range $\beta < 1$, the slope is nearly twice as large as compared to the range $\beta > 1$. Moreover, the reduced pressure P/P_{ideal} attains the values 0.77, 0.84, and 0.74 at $\beta = 0$, 1, and 2, respectively, demonstrating an increase of P/P_{ideal} in the first region and thereafter a decrease in the second one.

Obviously, the much larger increase of the osmotic pressure appearing in the range $\beta < 1$ is a consequence of the complexation between the macroions and the polyelectrolytes with the subsequent release of their counterions, whereas in the range $\beta > 1$ only a smaller fraction of the added counterions are osmotically active. The largest fraction of released counterions should appear at the macromolecular charge equivalence, and this is consistent with the maximum of reduced pressure appearing at $\beta \approx 1$.

3.2. Stoichiometric Charge Neutral System. Originating from the reference system at the stoichiometric charge ratio $\beta = 1$, the structure of systems with different (i) macroion size R_M, (ii) polyelectrolyte length N_{seg}, and (iii) bare chain persistence length l_p have been examined. Figure 8 shows typical configurations at different values of these parameters. The corresponding macroion−macroion structure factors and radial distribution functions at different R_M are given in Figures 9a and 10a, at different N_{seg} in Figures 9b and 10b, and at different l_p in Figures 9c and 10c.

3.2.1. Variation of Macroion Size. The structure of the systems at $R_M = 10$, 15, and 20 Å at constant macroion charge has been investigated. Figure 8a−c shows that the structure of the solution is strongly dependent on the macroion radius. A reduction from $R_M = 15$ (the reference system) to 10 Å leads to a compaction of the large cluster, whereas an increase to $R_M = 20$ Å results in a partial breakup of the cluster.

The macroion−macroion sf's given in Figure 9a display a larger magnitude at $0.05\ Å^{-1} < q < 0.1\ Å^{-1}$ for $R_M = 10$ Å as compared to $R_M = 15$ Å, consistent with a more compact cluster for the small macroion radius. At $R_M = 20$ Å, the amplitude at small q has decreased substantially, also consistent with the snapshots. The corresponding rdf's are given in Figure 10a. For $R_M = 10$, 15, and 20 Å, the locations of the first maximas are 25, 37, and 49 Å, respectively, giving surface-to-surface separations of 5, 7, and 9 Å, respectively, quantifying the formation of more compact clusters as R_M is decreased. In line with previous analyses, the nearest-neighbor peak vanishes (here for $R_M = 20$ Å) as the spatial correlation weakens.

Thus, despite the *stronger* macroion−macroion repulsion as R_M is reduced at fixed Z_M, neighboring macroions become closer to each other and the solution becomes destabilized. The attractive macroion−segment interaction is of course the driving force of the macroion−polyelectrolyte complexation, and consequently, the enforcement of the attractive macroion−segment interaction as R_M is reduced dominates over the increased macroion−macroion repulsion.

3.2.2. Variation of Polyelectrolyte Length. At $\beta = 1$, the reference system contains $N_{pe} = 10$ polyelectrolyte chains, each composed of $N_{seg} = 20$ charged segments in addition to the macroions and counterions. The structures of the systems with N_{seg} ranging from 5 to 40 have been investigated, keeping the total number of segments fixed at $N_{pe}N_{seg} = 200$. A comparison of the snapshots in Figure 8a,d indicates that a doubling of the number of segments per chain to $N_{seg} = 40$ does not strongly affect the clustering in the system, whereas a comparison of Figure 8a,e shows that a reduction to $N_{seg} = 5$ leads to a much weaker clustering.

The macroion−macroion sf's given in Figure 9b support the notion that the density fluctuations at short wave vectors are similar at $N_{seg} = 20$ and 40 but decrease as the length of the polyelectrolyte becomes smaller than $N_{seg} = 20$. At $N_{seg} = 5$, $S_{MM}(q)$ displays very little structuring, indicating that the macroions and polyelectrolytes form essentially neutral complexes with only weak interactions between the complexes and consistent with the snapshot given in Figure 8e. The corresponding rdf's are shown in Figure 10b. The magnitude of the maximum at $r \approx 37$ Å appearing from neighboring macroions is similar for $N_{seg} = 20$ and 40 and consistent with the sf data. As the polyelectrolyte chains are made shorter, the maximum is somewhat shifted outward, and its amplitude is strongly reduced. In addition, the second maximum appearing at $r \approx 65$ Å is shifted to longer separation and eventually vanishes as N_{seg} is reduced further.

Thus, the ability to form extended macroion−polyelectrolyte clusters is reduced as the polyelectrolyte length (and charge) is reduced. The reduced propensity of cluster formation as N_{seg} is decreased is also a

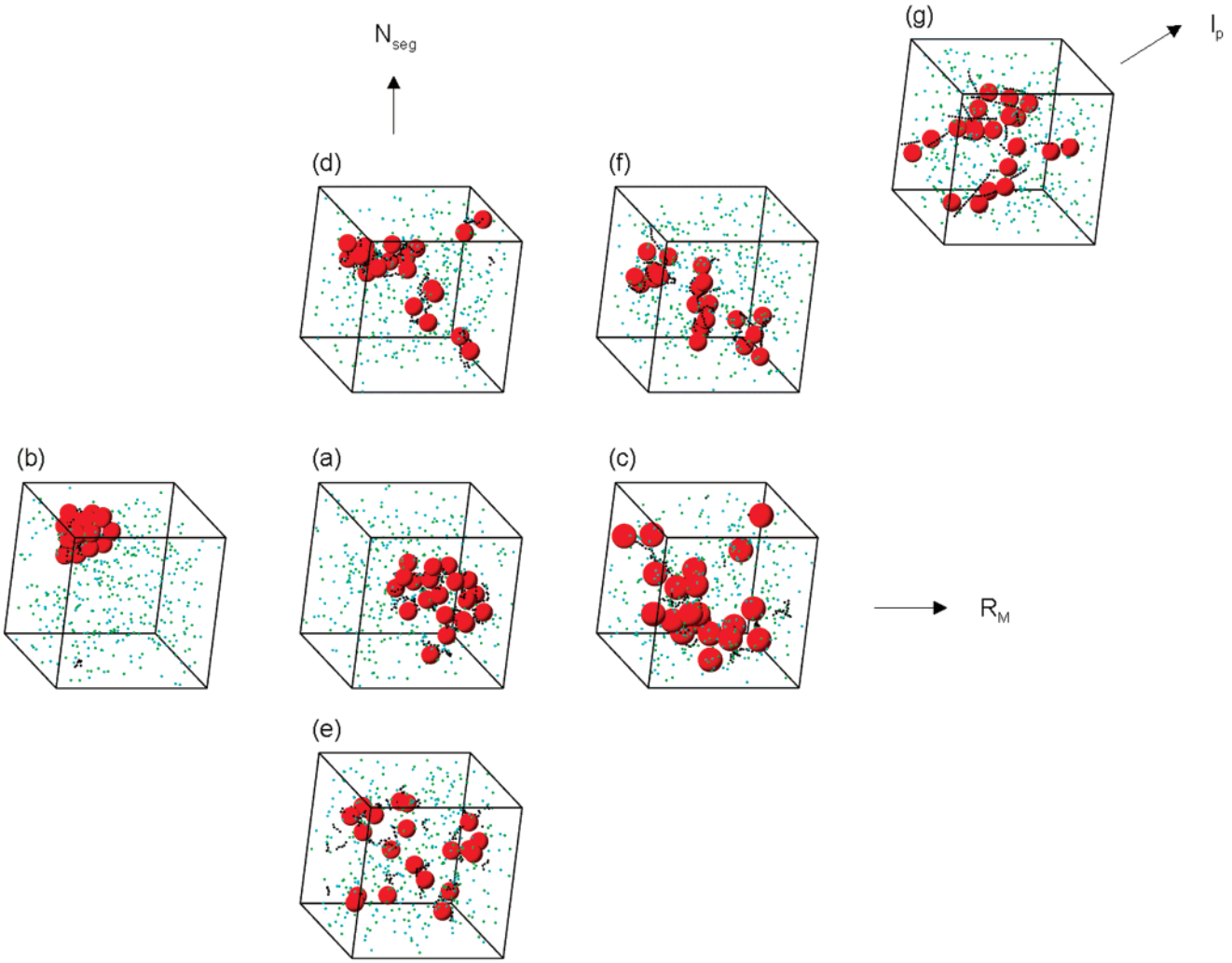

Figure 8. Typical configurations for different solutions of macroions and oppositely charged polyelectrolytes at the stoichiometric charge ratio $\beta = 1$. The systems are (a) the reference system (Table 1) and the reference system but (b) $R_M = 10$ Å, (c) $R_M = 20$ Å, (d) $N_{pe} = 5$ and $N_{seg} = 40$, (e) $N_{pe} = 40$ and $N_{seg} = 5$, (f) $l_p = 42$ Å, and (g) $l_p = 1480$ Å. Color coding as in Figure 2.

consequence of a change of the macroion−polyelectrolyte interaction. As the chain length and the net charge are reduced, the attractive macroion−polyelectrolyte segment interaction *per chain* is reduced, and the ability of a polyelectrolyte chain to bring macroions together is diminished. In the limit $N_{seg} = 1$, a solution of like-charged macroions with simple 1:1 salt added is recovered; in this solution and at the present conditions an effective repulsion would appear between two macroions.

3.2.3. Variation of Bare Chain Persistence Length. The structural changes of the system containing polyelectrolytes with the bare persistence lengths $l_p = 42$, 164, and 1480 Å, in addition to $l_p = 7$ Å in the reference system, will now be examined. With $l_p = 1480$ Å the persistence length becomes much longer than the contour length, making the chains behaving as rigid rods. The snapshots of the systems with $l_p = 7$, 42, and 1480 Å are given in parts a, f, and g of Figure 8, respectively. In all the three systems, considerable clustering appears, and for semiflexible chains ($l_p = 42$ Å), numerous and compact complexes are visible, while for rigid rods ≈2.5 elongated and loosely packed clusters are formed.

The macroion−macroion sf's given in Figure 9c display a *nonmonotonic* trend at small q as the persistence length is increased. The smallest amplitude is obtained with $l_p = 42$ Å; hence, the tendency for forming large clusters is weakest at an intermediate persistence length and larger for flexible and for very rigid polyelectrolytes. The corresponding macroion−macroion rdf's displayed in Figure 10c also show a nonmonotonic behavior with respect to a variation of l_p. At $l_p = 42$ Å, the tendency of forming macroion pairs is smallest and the amplitude at $r \approx 60-80$ Å is strongly reduced, as compared to more flexible or to more rigid polyelectrolytes, supporting the smaller probability of forming extended clusters. Hence, the quantitative analyses provided by the sf's and rdf's confirm the nonmonotonic variation of the cluster formation ability displayed by the snapshots.

The robustness of the nonmonotonic behavior of the solution stability as l_p is varied was examined by considering the macroion−macroion structure factors at different (i) ionic strength, (ii) macroion number density, and (iii) $|Z_{pe}/Z_M|$ ratios. In the reference system, the counterions to the macromolecules give rise to a Debye screening length of $\lambda_D = 22$ Å. Simulations of the reference system but without counterions, which is possible since $N_{cation} = N_{anion}$ in the reference system, were performed. The values of $S_{MM}(q)$ at $q = 0.024$ Å^{-1} became 9.5, 7.9, and 11.0 for $l_p = 7$, 42, and 1480 Å, respectively. Thus, in the absence of small ions the nonmonotonic trend remains, although less pronounced,

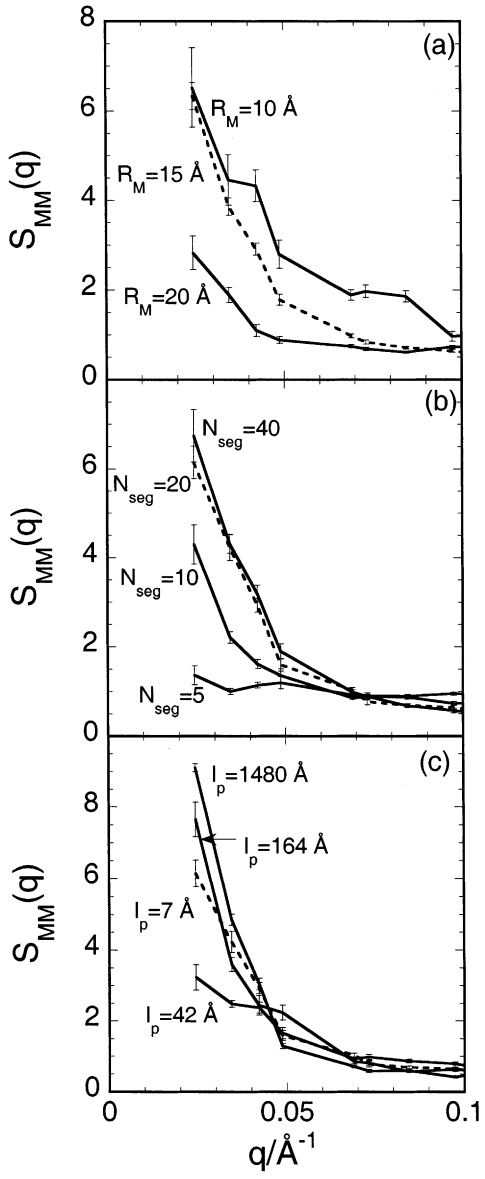

Figure 9. Macroion−macroion structure factors $S_{MM}(q)$ at the stoichiometric charge ratio $\beta = 1$ at indicated (a) macroion radius, (b) chain length, and (c) chain flexibility. Other parameters as in the reference system; see Table 1.

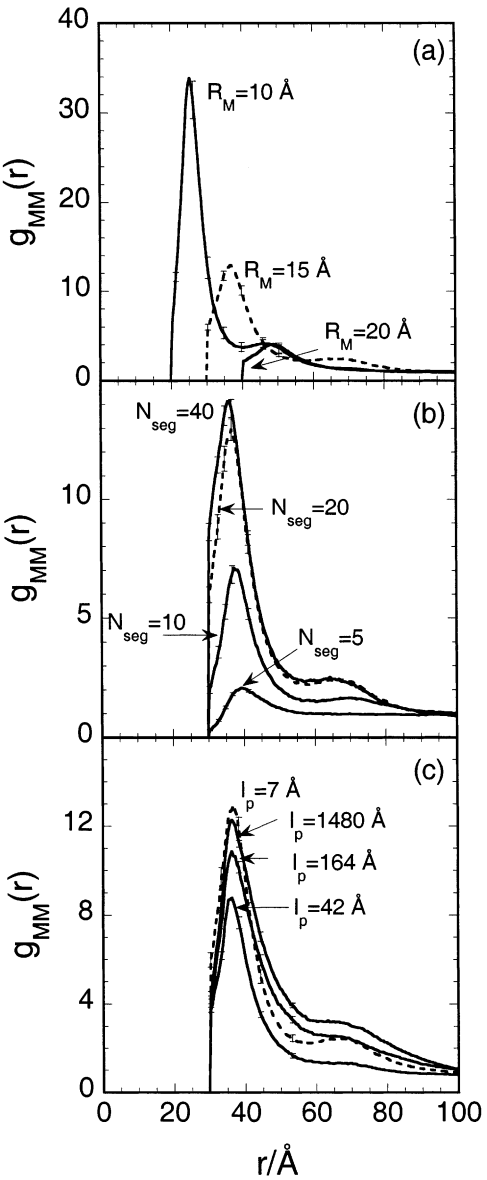

Figure 10. Macroion−macroion radial distribution functions $g_{MM}(r)$ at the stoichiometric charge ratio $\beta = 1$ at indicated (a) macroion radius, (b) chain length, and (c) chain flexibility. Other parameters as in the reference system; see Table 1.

and the values of S_{MM} at small q are increased due to the stronger (less screened) electrostatic interactions among the charged macromolecules. Second, the solution volume was increased by 60%. The corresponding values of the macroion−macroion structure factor became 5.4, 3.4, and 8.5, respectively, and again the nonmonotonic trend remains. Finally, investigations were performed with different ratio of the charge of a single polyelectrolyte to the charge of a single macroion $|Z_{pe}/Z_M|$. Hayashi et al.[42] have previously found that the propensity of a solution of oppositely charged polyelectrolytes to phase separate was suppressed when the polyelectrolytes carry the same absolute charge. Table 4 summarizes our findings, and the values of $S_{MM}(q)$ at small q again display that the least unstable solution is obtained at the intermediate bare persistence length l_p = 42 Å. To conclude, the nonmonotonic trend in Figure 9c appears at other screening lengths, macroion densities, and charge ratios $|Z_{pe}/Z_M|$, and hence it appears to be of substantial generality.

Table 4. $S_{MM}(q)$ at Small q[a]

$\|Z_{pe}\|$	$\|Z_{pe}/Z_M\|$	l_p = 7 Å	l_p = 42 Å	l_p = 1480 Å
10	1	3.1	1.5[b]	1.9[b]
20	2	6.25	3.5	9
25	2.5	7.4	4.2	8.8

[a] q = 0.024 Å^{-1}. [b] The structure factors display a maximum at q > 0.24 Å^{-1}, indicating repulsive interaction between clusters/complexes.

We will now make the conjecture that the smaller tendency to phase separate with the semiflexible chain as compared to the flexible and stiff ones is connected to the similar size of the bare persistence length l_p of the chain and the radius R_M of the macroion in the former case. In the following, we will use results from simpler systems to support this conjecture.

Consider a system containing a single polyelectrolyte and an oppositely charged macroion with their counterions confined in a finite volume. Figure 11 displays snapshots and the complexation probability $P_M^c(i_{seg})$ for this system for the bare persistence lengths l_p = 7, 42,

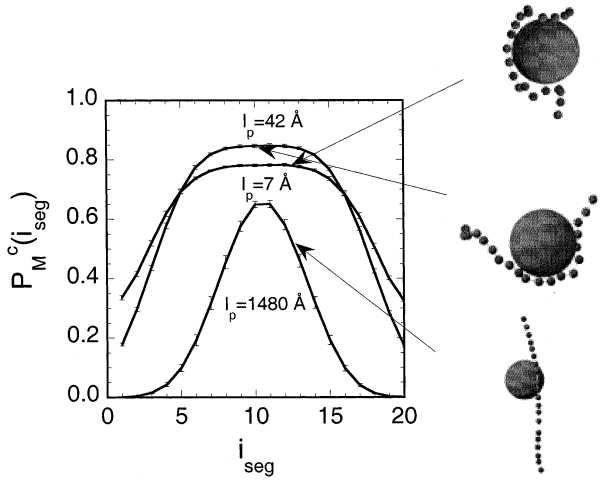

Figure 11. Typical configurations and complexation probability $P_M^c(i_{seg})$ vs segment rank i_{seg} with $N_{pe} = 1$, $N_M = 1$, $N_{cation} = 10$, and $N_{anion} = 20$ with $l_p = 7$, 42, and 1480 Å. Other parameters as in the reference system; see Table 1. In the snapshots, the small positive and negative ions are omitted for clarity.

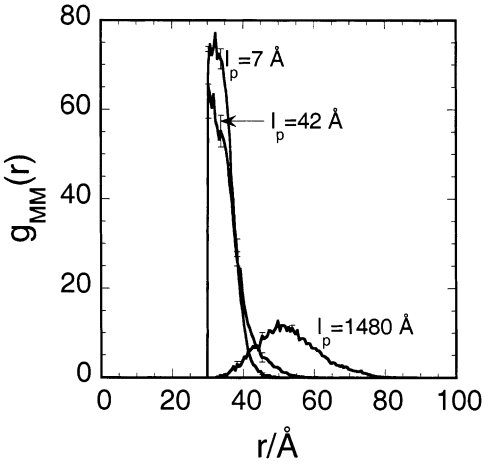

Figure 12. Macroion−macroion radial distribution functions $g_{MM}(r)$ for systems characterized by $N_{pe} = 1$, $N_M = 2$, $N_{cation} = 20$, and $N_{anion} = 20$ with $l_p = 7$, 42, and 1480 Å. Other parameters as in the reference system; see Table 1.

and 1480 Å. The snapshots show that the flexible (l_p = 7 Å) and semiflexible (l_p = 42 Å) chains are wrapped around the macroion, whereas the stiff chain (l_p = 1480 Å) only touches the macroion with a few segments. Moreover, the flexible chain displays small loops protruding from the surface, whereas for the semiflexible chain the surface layer is smooth. The complexation probabilities provide the probability that a given segment of the polyelectrolyte is complexed to the macroion.[32] The same geometrical criterion as above is used for defining a segment being complexed to the macroion. The trend observed is that the macroion prefer to complex to the central segments of the polyelectrolyte. [For the case $|Z_{pe}| \gg |Z_M|$, there are conditions where the macroion is complexed to one of the ends of the polyelectrolyte.[24,31,43]] The integral of the complexation probability function provides the average number of segments complexed to the macroion and becomes 12.5, 12.5, and 4.7 for the three l_p, respectively. Moreover, the binding region for the semiflexible chain is narrower and has a higher amplitude than for the flexible one, showing that the semiflexible chain creates a more compact surface layer than the flexible chain as was inferred from the snapshots. Hence, the structure of the complex formed between one macroion and one polyelectrolyte depends decisively on the bare persistence length of the polyelectrolyte at fixed macroion radius.

Corresponding simulations of systems containing one polyelectrolyte, two macroions, and their counterions with the same set of bare chain persistence lengths have also been performed. In this case, we have charge neutral complexes. The macroion−macroion rdf's of these systems are presented in Figure 12. For the flexible chain a pronounced maximum appears at r = 32 Å, whereas for the semiflexible chain the slightly lower maximum is located at the contact separation r = 30 Å. Regarding the stiff chain, the typical macroion separation is ≈50 Å, and the peak is much wider and displays a smaller amplitude. From these observations, we conclude that the two macroions complexed to one polyelectrolyte (i) are spatially near each other and hence are substantially electrostatically screened when the charged chain is flexible or semiflexible, (ii) whereas the macroions are substantially separated and hence less screened in the case of the rigid chain. Similar results with $N_{pe} = 1$, $N_M = 4$, and $|Z_{pe}/Z_M| = 4$ have previously been reported.[33]

To support our conjecture, we start with the observation that (i) the most compact surface layer appears when the chain persistence length is of the order of the macroion radius (Figure 11). Second, we argue that (ii) the weakest electrostatic attraction between two neutral complexes appears when the surface layer is compact. With either loops or extended tails present, segments in these parts of a chain are able to bridge to other macroions in neighboring complexes (Figures 11 and 12). Such an electrostatically driven bridging should be feasible, since polyelectrolyte segments cover only a small fraction of the macroion surface. Moreover, we found it most likely that (iii) the propensity of forming larger clusters and phase separation is related to the appearance of electrostatic attraction between neutral complexes. Finally, the combination of issues i−iii now leads to a support of our conjecture how the $l_p - R_M$ relationship affects the phase stability. The proposed mechanism is illustrated in Figure 13.

4. Conclusions

A simple model has been employed to investigate properties of polyelectrolyte−macroion solution by means of Monte Carlo simulations. It is expected that the physicochemical properties of such systems are dominated by the strong electrostatic attraction between the oppositely charged macromolecules, and hence the model has been designed with focus on the electrostatic interactions.

The phase stability of the macroion solution at increasing number of polyelectrolyte chains at fixed volume and at variable volume at fixed stoichiometric polyelectrolyte charge-to-macroion charge ratio has been examined. Structural analyses showed that as polyelectrolytes are added the system undergoes a sequence of states: homogeneous macroion solution → stable solution containing macroion−polyelectrolyte complexes → two-phase system comprising of one phase rich in the macromolecules and one poor in them → a single and stable macroion−polyelectrolyte solution (redissolution). Despite the limited amount of data, the phase behavior of the model system displays salient features appearing in corresponding experimental systems: a closed two-

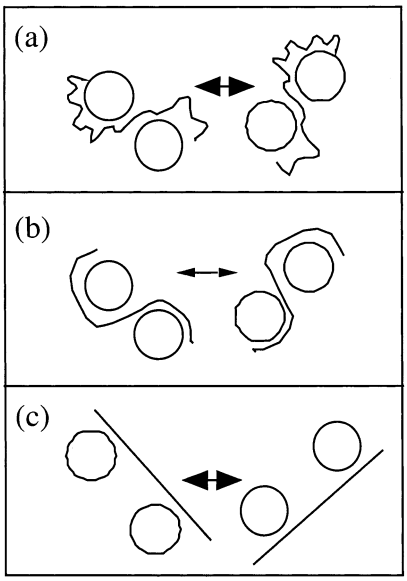

Figure 13. Schematic drawing showing two stoichiometric charge neutral complexes, each containing one polyelectrolyte and two macroions for (a) flexible, (b) semiflexible, and (c) stiff polyelectrolytes, and the stronger attractive interaction between the two such complexes with either flexible or stiff polyelectrolytes (thicker arrows).

phase region extending along the line of macromolecular charge equivalence line and terminating at low water content and at extremely high dilution. The high dilution limit was not reached, but the system has to become homogeneous by entropic reasons in this limit. We also notice that there is generally a qualitative agreement between recent theoretical predictions[35−37] and the properties of the model system under investigation.

We have previously observed that polyelectrolyte−macroion complexation is accompanied by a release of counterions from the vicinity of the charged macromolecules. Here, this release was monitored by an examination of the osmotic pressure. Indeed, the osmotic pressure as a function of the amount of polyelectrolyte added displayed a break and the reduced osmotic pressure possessed a maximum at macromolecular charge equivalence—in agreement with the notion of a maximal release of counterions at this condition.

Moreover, it was observed that the propensity of phase separation increased as the macroions were made smaller at fixed charge and as the polyelectrolytes were made longer. In addition, the tendency for phase separation was smaller for a semiflexible chain and larger for flexible and rigid chains. We observed that thinnest adsorbed polymer layer is obtained when the chain persistence length is similar to the macroion radius, and we argue that the neutral complex formed by appropriate amount of such semiflexible polyelectrolytes and macroions possess the smallest tendency to electrostatically attract other similar complexes and therefore displays a weaker tendency to phase separate.

Acknowledgment. M. Skepö thanks Magnus Ullner for valuable discussions. The work was supported by grants from the Foundation of Strategic Research (SSF), through National Graduate School in Scientific Computing (NGSSC), the Swedish Research Council for Engineering Science (TFR), the Swedish National Research Council (NFR), and by computing resources by the Swedish Council for Planning and Coordination of Research (FRN) and the National Supercomputer Centre (NSC), at Linköping University.

References and Notes

(1) Sukhorukov, G. B.; Donath, E.; Davis, S.; Lichtenfield, H.; Caruso, F.; Popov, V. I.; Möhwald, H. *Polym. Adv. Technol.* **1998**, *9*, 759.
(2) *Polymer-Surfactant Systems*; Kwak, J. C. T., Ed.; Marcel Dekker: New York, 1998; Vol. 77.
(3) Tsuboi, A.; Izumi, T.; Hirata, M.; Xia, J.; Dubin, P. L.; Kokufuta, E. *Langmuir* **1996**, *12*, 6295.
(4) Xia, J.; Dubin, P. L. Protein-Polyelectrolyte Complexes. In *Macromolecular Complexes in Chemistry and Biology*; Dubin, P., Bock, J., Davis, R., Schulz, D. N., Thies, C., Eds.; Springer-Verlag: Berlin, 1994.
(5) Ganachaud, F.; Elaïssari, A.; Pichot, C.; Laayoun, A.; Cros, P. *Langmuir* **1997**, *13*, 701.
(6) Bielinska, A. U.; Chen, C.; Johnson, J.; Baker, J. R. *Bioconjugate Chem.* **1999**, *10*, 843.
(7) Luger, K.; Mader, A. W.; Richmond, R. K.; Sarget, D. F.; Richmond, T. J. *Nature (London)* **1997**, *389*, 251.
(8) Widom, J. *Annu. Rev. Biophys. Biomol. Struct.* **1998**, *27*, 258.
(9) *Colloid Science*; Bungenberg de Jong, H. G., Ed.; Elsevier: Amsterdam, 1949; Vol. 2.
(10) Guillemet, F.; Piculell, L. *J. Phys. Chem.* **1995**, *99*, 9201.
(11) Ilekti, P.; Piculell, L.; Tournilhac, F.; Cabane, B. *J. Phys. Chem. B* **1998**, *102*, 344.
(12) Lindman, B.; Thalberg, K. Polymer-surfactant interactions—recent developments. In *Interactions of Surfactants with Polymers and Proteins*; Goddard, E. D., Ananthapadmanabhan, K. P., Eds.; CRC Press: Boca Raton, FL, 1993; p 203.
(13) Piculell, L.; Lindman, B. *Adv. Colloid Interface Sci.* **1992**, 149.
(14) Ranganathan, S.; Kwak, J. C. T. *Langmuir* **1996**, *12*, 1381.
(15) Goddard, E. D.; Hannan, R. B. *J. Am. Oil Chem. Soc.* **1977**, *54*, 561.
(16) Ohbu, K.; Hiraishi, O.; Kashiwa, I. *J. Am. Oil. Chem. Soc.* **1982**, *59*.
(17) Thalberg, K.; Lindman, B. *J. Phys. Chem.* **1989**, *93*, 1478.
(18) Thalberg, K.; Lindman, B.; Bergfeldt, K. *Langmuir* **1991**, *7*, 2893.
(19) Thalberg, K.; Lindman, B.; Karlström, G. *J. Phys. Chem.* **1991**, *95*, 3370.
(20) Carnali, J. O. *Langmuir* **1993**, *9*, 2933.
(21) von Goeler, F.; Muthukumar, M. *J. Chem. Phys.* **1994**, *100*, 7796.
(22) Gurovitch, E.; Sens, P. *Phys. Rev. Lett.* **1999**, *82*, 339.
(23) Park, S. Y.; Bruinsma, R. F.; Gelbart, W. M. *Europhys. Lett.* **1999**, *46*, 454.
(24) Mateescu, E. M.; Jeppesen, C.; Pincus, P. *Europhys. Lett.* **1999**, *46*, 493.
(25) Netz, R.; Joanny, J.-F. *Macromolecules* **1999**, *32*, 9013.
(26) Nguyen, T. T.; Shklovskii, B. I. *Physcia A* **2001**, *293*, 324.
(27) Chodanowski, P.; Stoll, S. *Macromolecules* **2001**, *34*, 2320.
(28) Chodanowski, P.; Stoll, S. *J. Chem. Phys.* **2001**, *115*, 4951.
(29) Akinchina, A.; Linse, P. *Macromolecules* **2001**, *35*, 5183.
(30) Nguyen, T. T.; Shklovskii, B. I. *J. Chem. Phys.* **2001**, *114*, 5905.
(31) Schiessel, H.; Bruinsma, R.; Gelbart, W. M. *J. Chem. Phys.* **2001**, *115*, 7245.
(32) Jonsson, M.; Linse, P. *J. Chem. Phys.* **2001**, *115*, 3406.
(33) Jonsson, M.; Linse, P. *J. Chem. Phys.* **2001**, *115*, 10975.
(34) Skepö, M.; Linse, P. *Phys. Rev. E*, in press.
(35) Ferreira, P. G.; Dymitrowska, M.; Belloni, L. *J. Chem. Phys.* **2000**, *113*, 9849.
(36) Nguyen, T. T.; Shklovskii, B. I. *J. Chem. Phys.* **2001**, *115*, 7298.
(37) Harnau, L.; Hansen, J.-P. *J. Chem. Phys.* **2002**, *116*, 9051.
(38) Allen, M. P.; Tildesley, D. J. *Computer Simulations of Liquids*; Oxford University Press: New York, 1987.
(39) Binder, K. *Monte Carlo and Molecular Dynamics Simulations in Polymer Science*; Oxford University Press: New York, 1995.
(40) Linse, P. *MOLSIM*, Version 3.0; Lund University: Sweden, 1999.
(41) Thalberg, K.; Lindman, B.; Karlström, G. *J. Phys. Chem.* **1991**, *95*, 6004.
(42) Hayashi, Y.; Ullner, M.; Linse, P. *J. Phys. Chem. B*, submitted.
(43) Akinchina, A.; Linse, P. *J. Phys. Chem. B*, submitted.

MA020634L